

Mohammad Vasef

The vast majority of the non-hematolymphoid neoplasms in the bone marrow are metastatic in nature (Figs. 18.1, 18.2, 18.3, 18.4, 18.5, 18.6, 18.7, 18.8, 18.9, 18.10, 18.11, 18.12, 18.13, 18.14, 18.15, 18.16, 18.17, 18.18, 18.19, 18.20, 18.21, 18.22, 18.23, 18.24, 18.25, 18.26, 18.27, 18.28, 18.29, 18.30, 18.31, 18.32, 18.33, 18.34, 18.35, 18.36, 18.37, and 18.38). Accurate diagnosis and subtyping require careful histomorphologic examination with integration of immunohistochemical results and, in certain cases, cytogenetics and molecular genetic findings.

The incidence of bone marrow metastasis varies significantly among different tumors. Tumors with the highest frequency of bone marrow metastasis include carcinomas of the breast (Figs. 18.1, 18.2, 18.3, 18.4, 18.5, 18.6, and 18.7), prostate (Figs. 18.18, 18.19, 18.20, and 18.21), gastrointestinal tract (Figs. 18.16, 18.17), and lung (Figs. 18.8, 18.9, 18.10, and 18.11) in adults and neuroblastoma (Figs. 18.24, 18.25, 18.26, 18.27, 18.28, and 18.29) in the pediatric age group. The published incidence of bone marrow metastasis for a given tumor differs significantly because of variability in techniques used to assess the bone marrow, as well as differences in patient selection. Studies using only bone marrow aspirate most likely have underestimated the true incidence of metastatic disease in bone marrow. Highly sensitive detection methods for circulating tumor cells can detect very low levels of disseminated tumor cells in patients with breast cancer and other types of cancer—much lower than can be identified by routine microscopic examination. The clinical significance of this very low-level involvement has been debated, however.

Carcinoma of the breast is the most common metastatic disease detected in the bone marrow in women. Prostate and

lung carcinomas are the most common metastatic diseases among men. Among all the histologic subtypes of lung cancer, small cell carcinoma has the highest incidence of bone marrow involvement. Other, less common tumors with bone marrow metastasis in adults include colon and gastric adenocarcinoma. Neuroblastoma has the highest incidence of bone marrow metastasis in children. Other tumors with a high incidence of marrow involvement in children include rhabdomyosarcoma (Figs. 18.36, 18.37, and 18.38), primitive neuroectodermal tumor (PNET)/Ewing sarcoma (Figs. 18.30, 18.31, 18.32, and 18.33), retinoblastoma (Figs. 18.34, 18.35), and medulloblastoma.

Circulating tumor cells are rarely detected in peripheral blood smears, particularly at the feather edge of the smear. Typically, these are seen in small clusters or are singly distributed and may mimic lymphoma cells.

Histomorphologic assessment of bone marrow is important in the staging of a newly diagnosed solid tumor or in monitoring of disease and therapeutic response. Trephine biopsy is crucial in assessing metastatic tumors because associated fibrosis renders most metastatic solid tumors unspirable. In addition, bilateral trephine biopsies may improve the diagnostic yield because of the patchy distribution of some metastatic tumors. Common metastatic tumors in children, including neuroblastoma, rhabdomyosarcoma, and Ewing sarcoma, are often present in both aspirate smears and trephine biopsy; however, in rare occasions only aspirate smears are diagnostic.

In rare circumstances, a bone marrow core biopsy or an image-guided bone biopsy may be performed to obtain tumor tissue for molecular genetic studies. In these circumstances, it is crucial to preserve the integrity of the DNA by avoiding strong, acid-based decalcification solution. A useful alternative would be EDTA-based solutions. Limited mutation-specific antibodies such as *BRAF* V600E or *EGFR* mutation-specific antibodies are available, which would work on tissues previously decalcified in strong, acid-based solutions.

M. Vasef (✉)

Department of Pathology, University of New Mexico Health Sciences Center, Albuquerque, NM, USA
e-mail: mvasef@salud.unm.edu

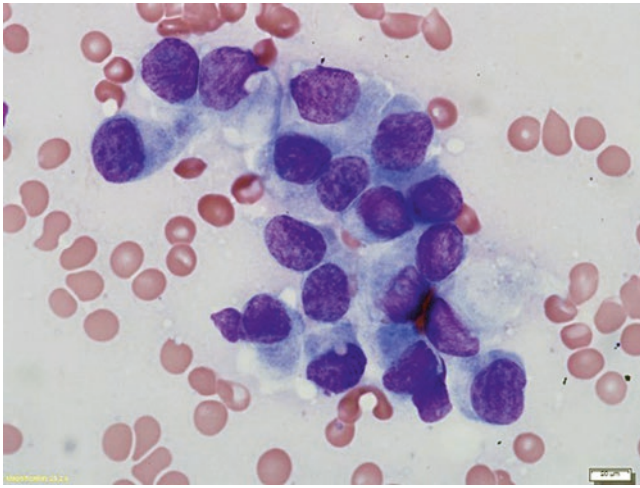


Fig. 18.1 Wright-stained touch imprint of a bone marrow trephine biopsy from a patient with a remote history of breast carcinoma shows a cluster of loosely cohesive metastatic carcinoma cells with large, oval nuclei and moderate amounts of wispy cytoplasm

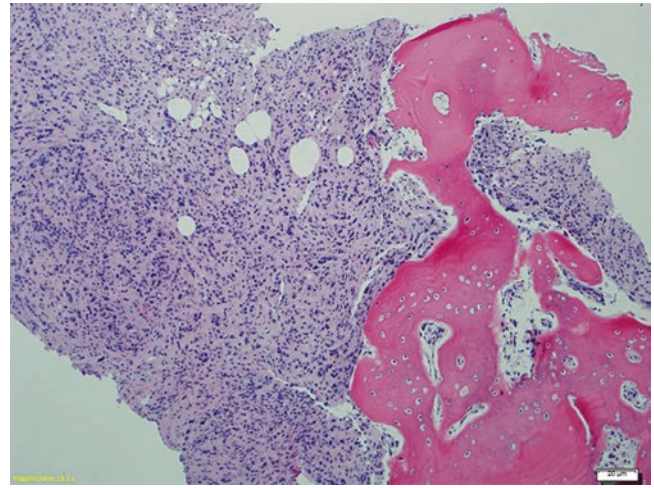


Fig. 18.3 Low-power view of an H&E-stained bone marrow trephine biopsy specimen demonstrates extensive involvement by metastatic lobular carcinoma of the breast. The patient had been diagnosed with stage II lobular carcinoma of the breast 10 years ago and had been treated with mastectomy and adjuvant chemotherapy. She now presents with anemia and leukopenia. Metastatic classic lobular carcinoma often tends to be distributed singly within the marrow space and may mimic a hematopoietic neoplasm

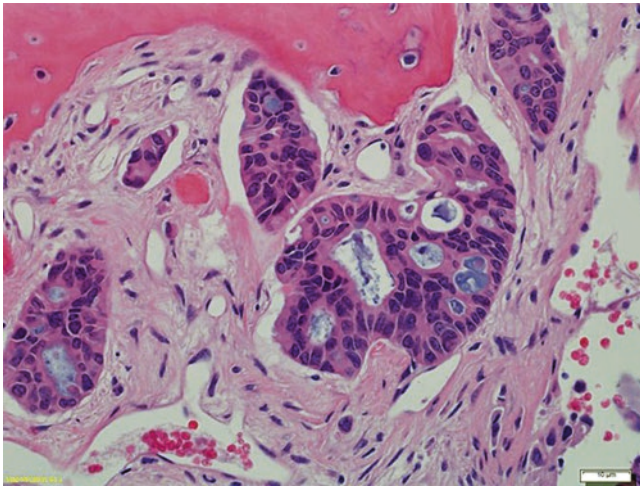


Fig. 18.2 Concurrent bone marrow trephine biopsy shows metastatic ductal carcinoma of breast primary with cribriform architecture similar to the histologic appearance of the tumor in the original breast site. Notice a component of intrasinusoidal tumor distribution, as well as a significant desmoplastic stromal response

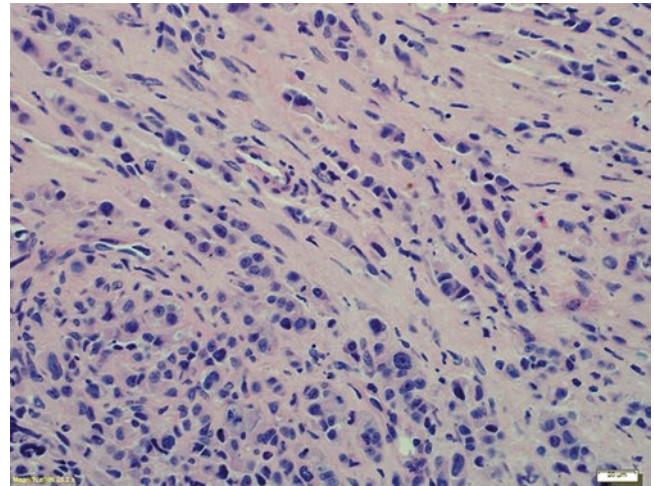


Fig. 18.4 High-power view of the bone marrow shows extensive bone marrow replacement by metastatic epithelial cells with intermediate-sized nuclei and scant to moderate amounts of cytoplasm. Notice the frequent single-file distribution typical of lobular breast carcinoma. Metastatic classic lobular carcinoma is often distributed singly within the bone marrow space, without a significant desmoplastic response, and can mimic a hematopoietic neoplasm

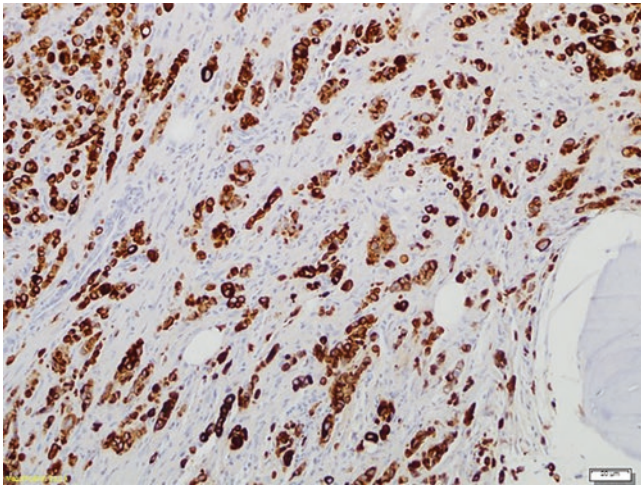


Fig. 18.5 Paraffin immunohistochemical stain using pankeratin antibody highlights the frequent single-file distribution, as well as individually distributed metastatic lobular carcinoma, in this bone marrow core biopsy specimen

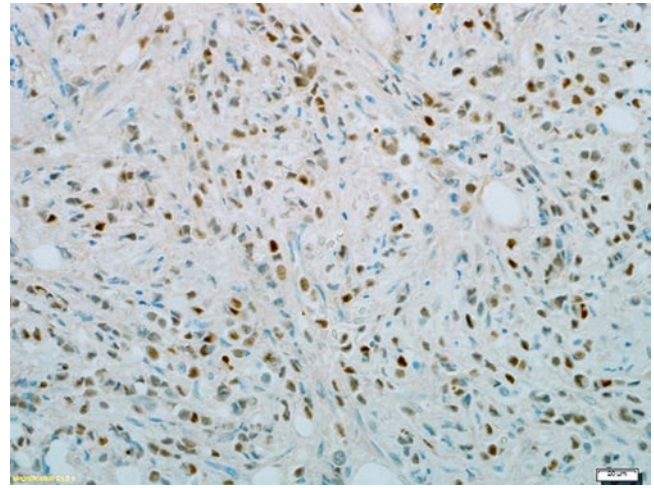


Fig. 18.7 Paraffin immunohistochemical stain using anti-estrogen receptor (anti-ER) antibody highlights metastatic carcinoma cells distributed singly within the bone marrow space in this example of metastatic classic lobular breast carcinoma

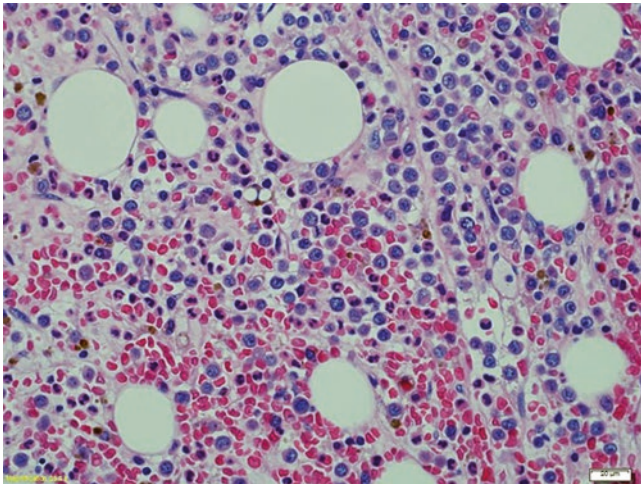


Fig. 18.6 High-power view of a bone marrow core biopsy involved by metastatic classic lobular breast carcinoma shows small neoplastic cells with regular nuclei distributed singly and interspersed among significantly decreased residual hematopoietic cells. In the absence of a prior clinical history of breast cancer and without ancillary studies, the classic lobular carcinoma can be erroneously interpreted as a hematopoietic malignancy

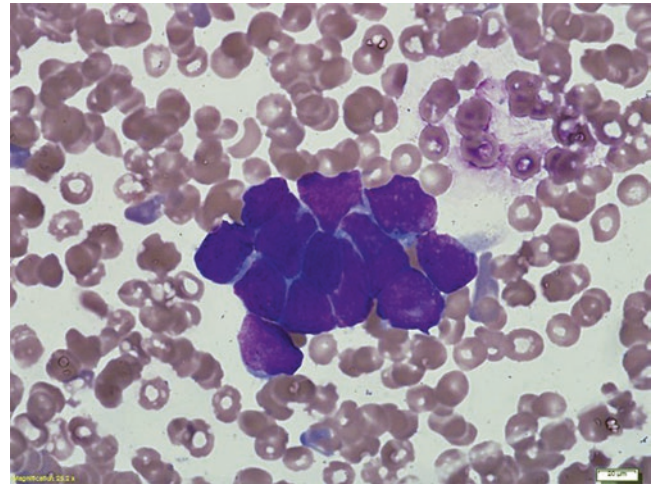


Fig. 18.8 Wright-stained bone marrow aspirate shows a cluster of cohesive tumor cells with a high nuclear-cytoplasmic (N:C) ratio, hyperchromatic nuclei, and nuclear molding from a patient with metastatic high-grade neuroendocrine small cell carcinoma of lung origin

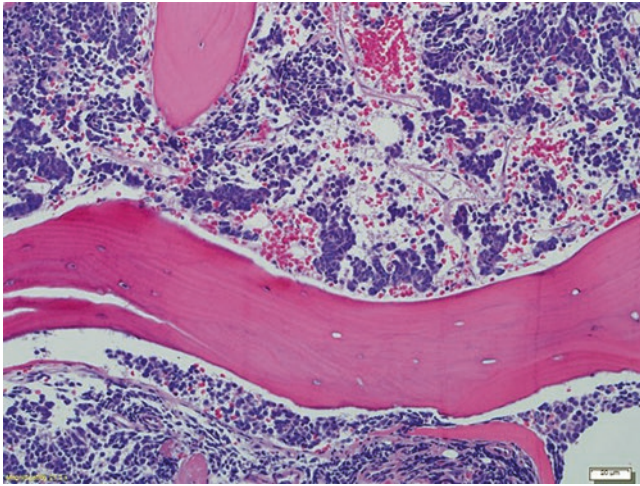


Fig. 18.9 H&E-stained bone marrow trephine biopsy shows extensive marrow involvement by metastatic small cell carcinoma of the lung

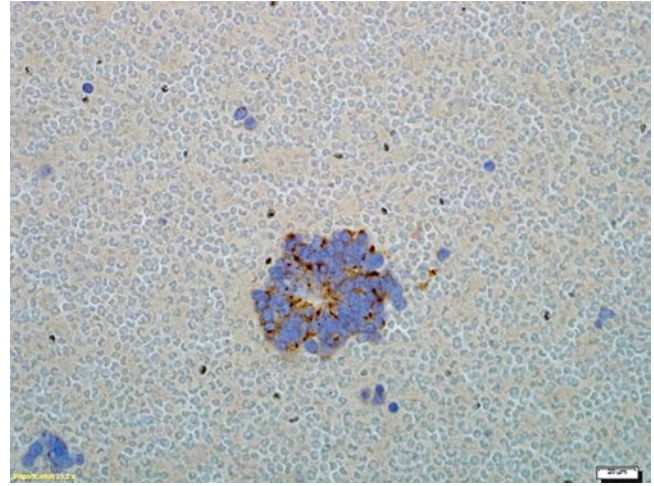


Fig. 18.11 Immunohistochemical stain using anti-chromogranin antibody performed on the marrow clot section highlights clusters of metastatic small cell carcinoma of the lung with a paranuclear, dotlike pattern of chromogranin expression

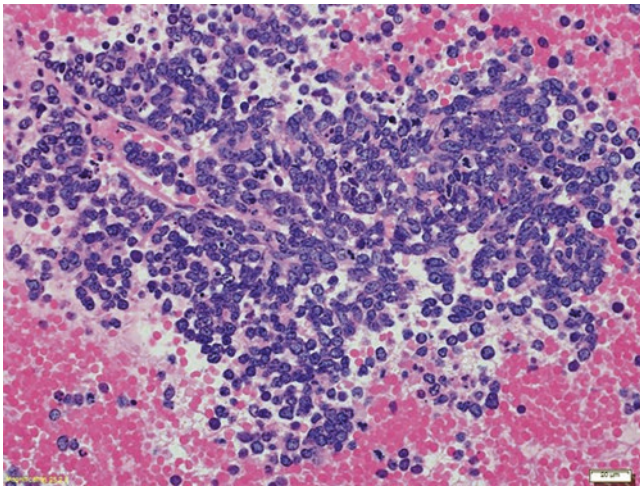


Fig. 18.10 H&E-stained histologic section of bone marrow clot section shows a large aggregate of metastatic small cell carcinoma of lung primary. The neoplastic cells show a so-called salt-and-pepper chromatin pattern with a high mitotic rate without a significant stromal response, which raises the differential diagnosis of a hematopoietic tumor or a sarcoma such as Ewing sarcoma

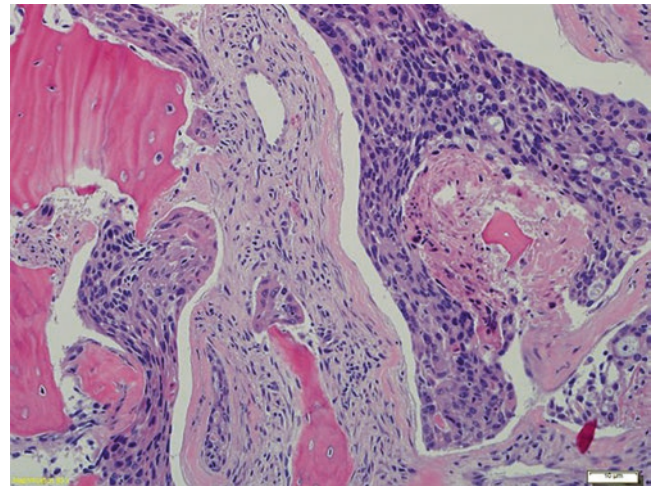


Fig. 18.12 This H&E-stained bone marrow trephine biopsy specimen from a 38-year-old woman with squamous cell carcinoma of the uterine cervix shows extensive intrasinusoidal involvement by metastatic deposits of poorly differentiated carcinoma. Extensive desmoplastic stromal reaction and prominent stromal fibrosis with focal bone resorption are also present

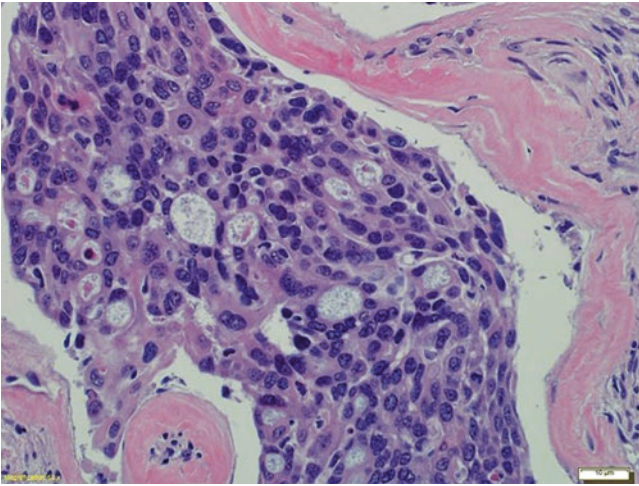


Fig. 18.13 The poorly differentiated metastatic carcinoma from the same patient as in Fig. 18.12, with metastatic squamous cell carcinoma of the uterine cervix, shows glandular differentiation and mucin production in this microscopic field

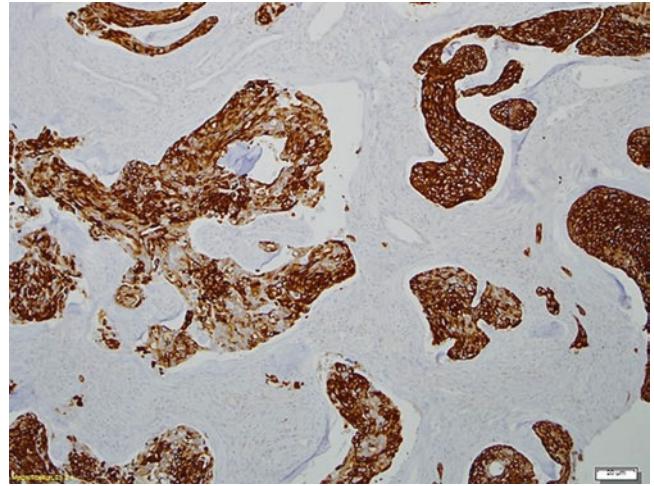


Fig. 18.15 Immunohistochemical stain performed on the bone marrow trephine biopsy reveals strong expression of keratin 5/6, supportive of metastatic squamous cell carcinoma in this poorly differentiated tumor

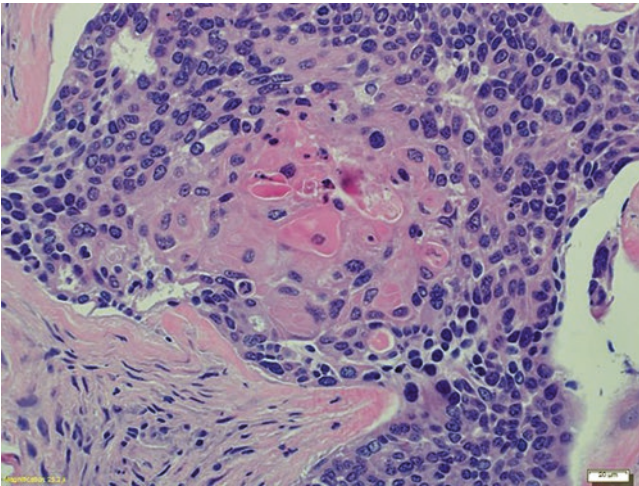


Fig. 18.14 The H&E-stained section of marrow core biopsy of the patient with metastatic squamous cell carcinoma shows focal keratinization in this field. Review of the histologic sections from the primary site similarly demonstrated foci of glandular differentiation and keratinization

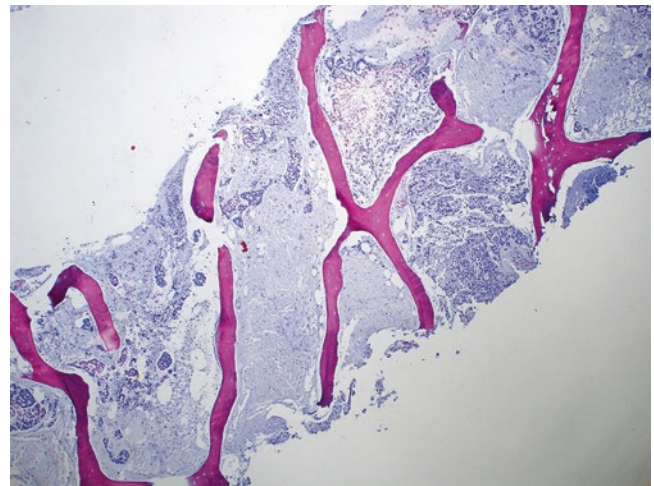


Fig. 18.16 H&E-stained section of bone marrow trephine biopsy from a 45-year-old patient with a history of metastatic mucinous adenocarcinoma of the colon reveals extensive acellular, mucinous material replacing the marrow space, with scattered clusters and aggregates of malignant cells within the mucinous pool

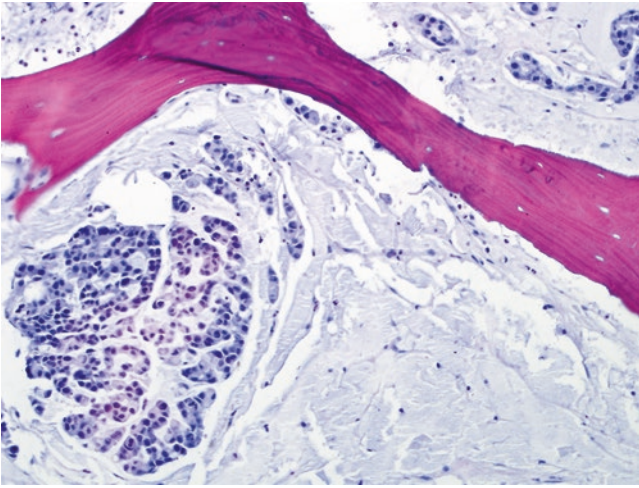


Fig. 18.17 H&E-stained high-power view of metastatic mucinous adenocarcinoma involving this bone marrow shows clusters of tumor cells with acinar and cribriform patterns floating free in pools of mucin

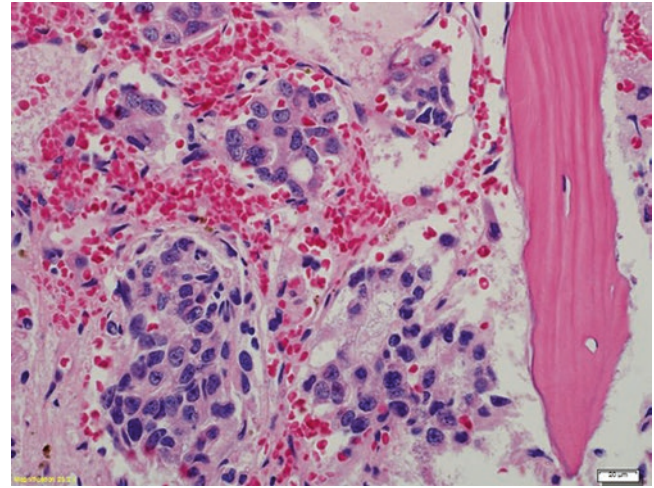


Fig. 18.19 Concurrent H&E-stained bone marrow trephine biopsy from the same patient as in Fig. 18.18 shows extensive marrow involvement by metastatic, well-differentiated prostatic adenocarcinoma with an intrasinusoidal distribution pattern

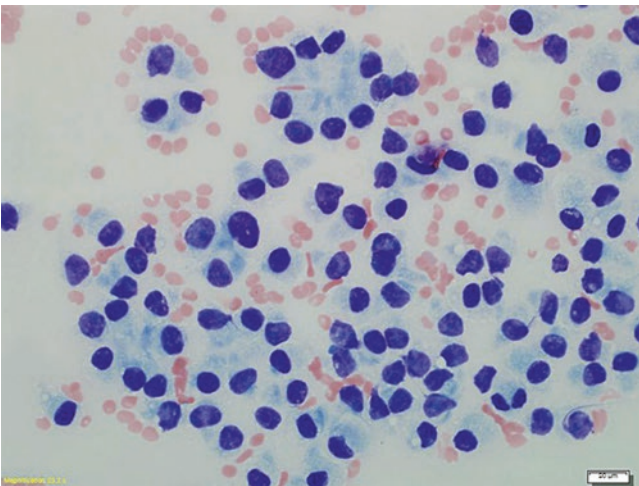


Fig. 18.18 Wright-stained bone marrow touch imprint from a patient with a history of prostatic carcinoma reveals a well-differentiated adenocarcinoma with acinar formation, consistent with marrow involvement by metastatic prostatic adenocarcinoma

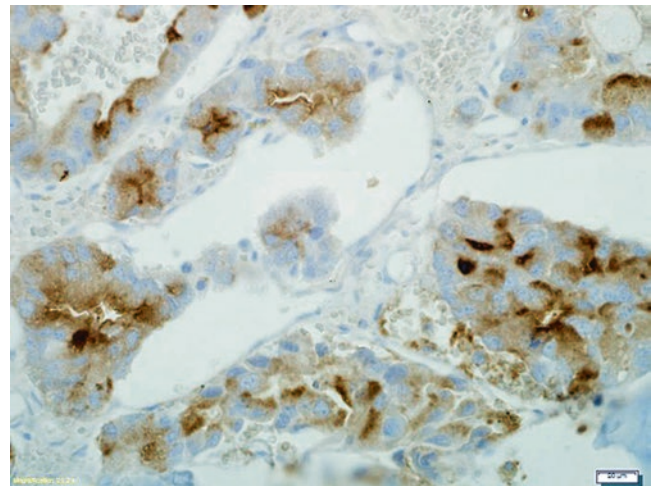


Fig. 18.20 Paraffin immunohistochemical stain using prostate-specific antigen (PSA) antibody marks neoplastic cells in this bone marrow biopsy involved by a moderately differentiated adenocarcinoma of prostatic origin

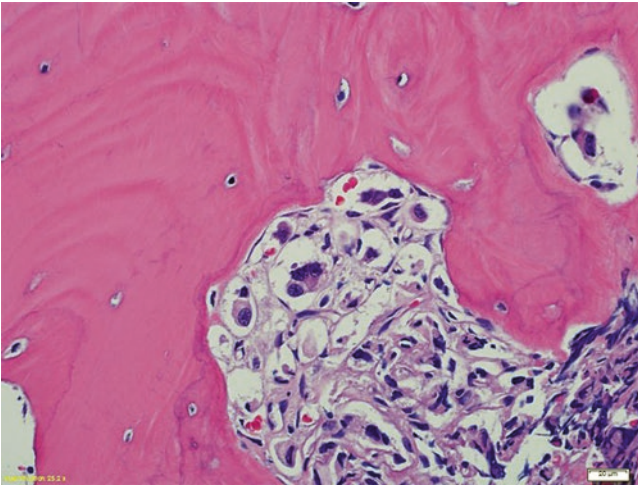


Fig. 18.21 H&E-stained bone marrow trephine biopsy with extensive involvement by a poorly differentiated prostatic adenocarcinoma with prominent bone sclerosis. Bone metastasis is common in prostate cancer and is typically associated with a sclerotic reaction

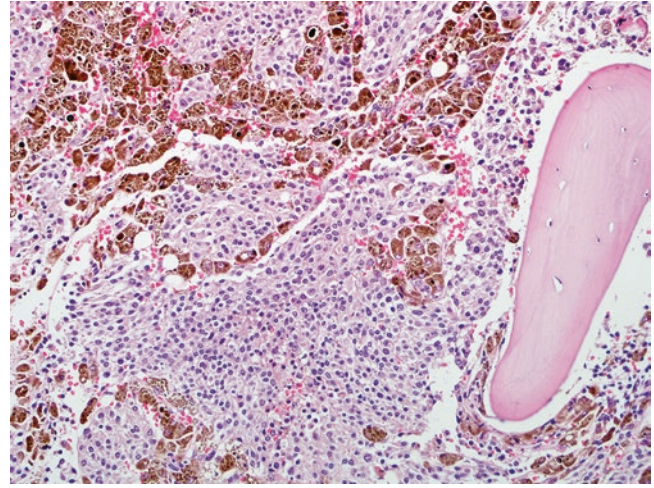


Fig. 18.23 High-power view of the bone marrow trephine biopsy shows extensive metastatic malignant melanoma replacing the marrow space. Abundant pigment-laden macrophages are also present, consistent with melanophages

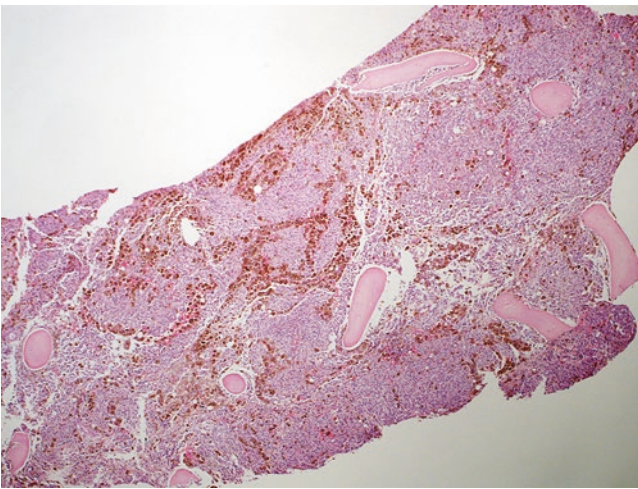


Fig. 18.22 Low-power view of a bone marrow core biopsy shows extensive involvement by metastatic malignant melanoma. Notice prominent pigment deposition

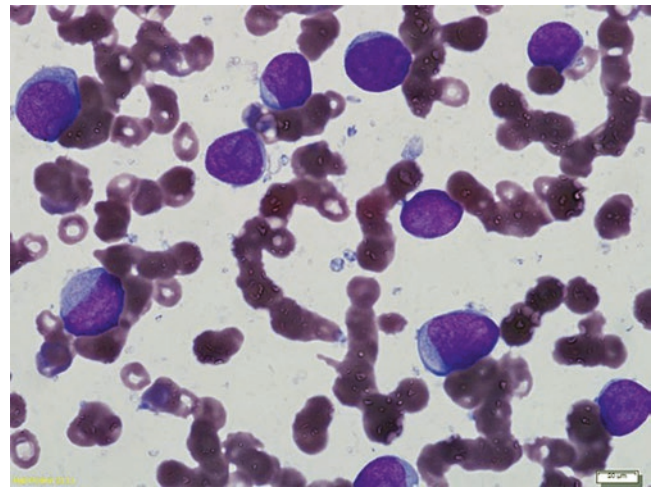


Fig. 18.24 Wright-stained bone marrow aspirate smear from an 11-year-old boy with a recent diagnosis of retroperitoneal neuroblastoma reveals singly distributed metastatic neuroblastoma cells with small, regular nuclei, occasional distinct nucleoli, and scant amounts of cytoplasm resembling lymphoblasts

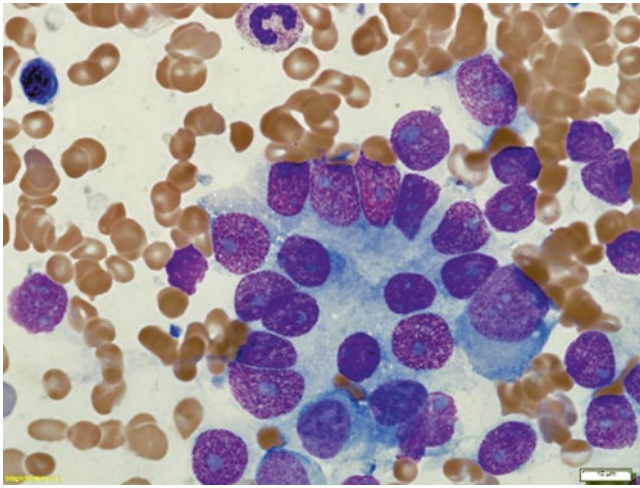


Fig. 18.25 This Wright-stained bone marrow aspirate smear from a child with metastatic neuroblastoma reveals tumor cells with partially degenerated, regular nuclei with prominent nucleoli and indistinct cytoplasmic borders surrounding fibrillary material consistent with a Homer Wright rosette formation

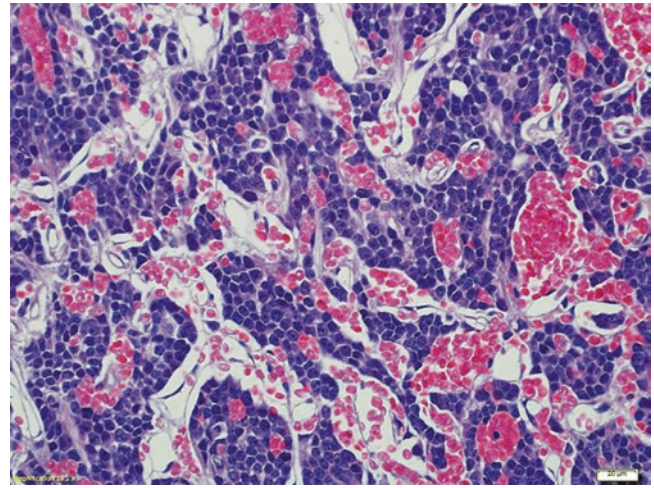


Fig. 18.27 High-power view of bone marrow trephine biopsy with extensive metastatic neuroblastoma reveals irregularly shaped, large aggregates of tumor cells surrounding dilated sinuses. There is markedly decreased trilineage hematopoiesis. Analysis using fluorescence in situ hybridization (FISH) revealed amplification of the *MYCN* gene, suggestive of a poor prognosis

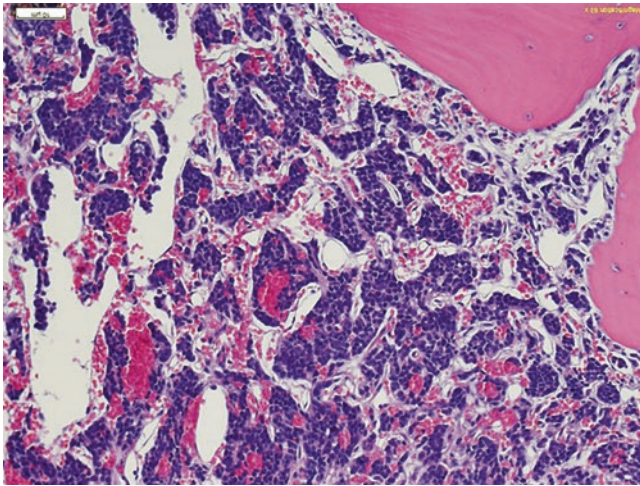


Fig. 18.26 H&E-stained staging bone marrow trephine biopsy from a child with a history of neuroblastoma reveals extensive marrow involvement by metastatic neuroblastoma distributed in compact aggregates of uniform and monotonous tumor cells

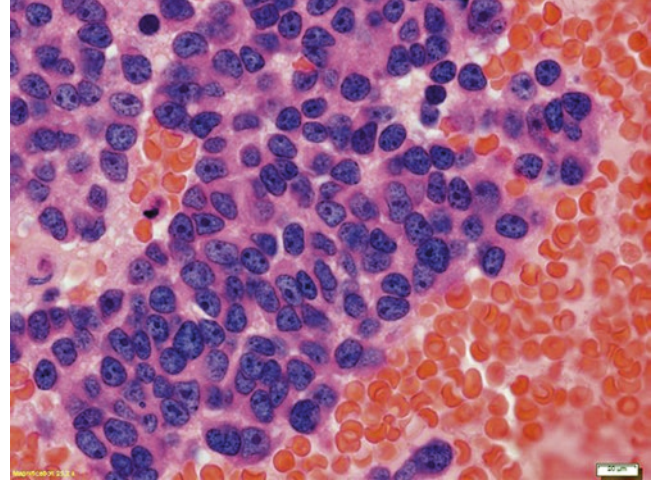


Fig. 18.28 H&E-stained bone marrow clot section from a child with stage IV neuroblastoma reveals aggregates of metastatic tumor cells with indistinct cytoplasmic borders in a background of fibrillary material, with occasional rosette formations

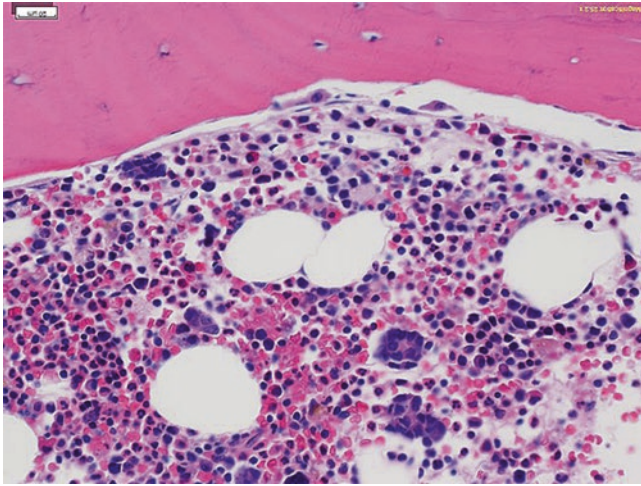


Fig. 18.29 This H&E-stained bone marrow trephine biopsy from a child with a history of stem cell transplantation and chimeric antibody therapy for high-stage neuroblastoma reveals a normocellular marrow with active hematopoiesis and minute foci of metastatic tumor cells, consistent with relapsed neuroblastoma

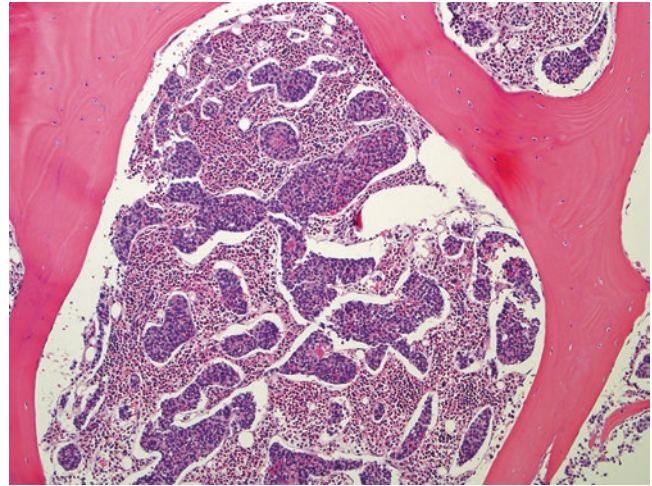


Fig. 18.31 H&E-stained low-power view of this bone marrow core biopsy shows extensive bone marrow involvement by Ewing sarcoma/PNET

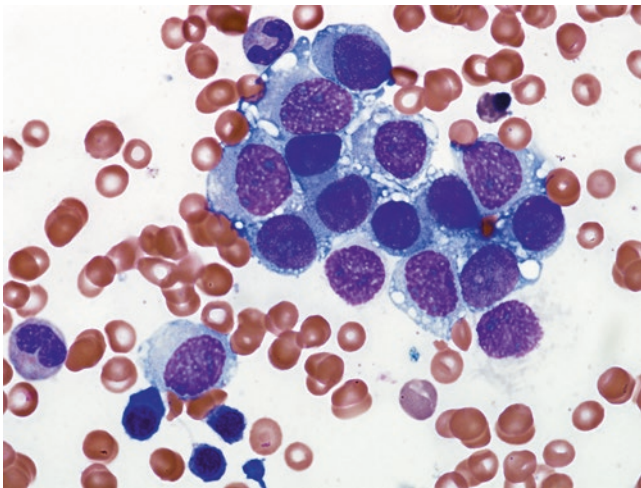


Fig. 18.30 Wright-stained bone marrow aspirate smear reveals a loose aggregate of small cells with round nuclei, finely dispersed chromatin, one or more small nucleoli, and scant cytoplasm. The tumor cells expressed FLI1 and CD99 by immunohistochemistry, and FISH analysis detected the *FLI1-EWS* fusion gene, supporting a diagnosis of Ewing sarcoma/primitive neuroectodermal tumor (PNET)

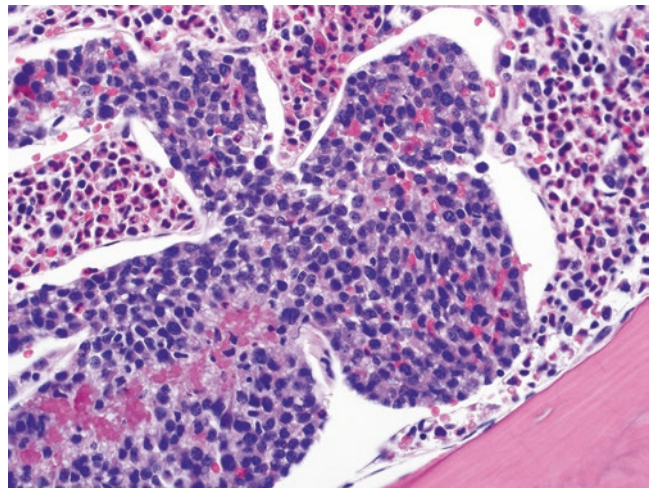


Fig. 18.32 High-power view of bone marrow core biopsy shows large aggregates of Ewing sarcoma associated with tumor necrosis in the center portion of the tumor aggregate. Ewing sarcoma frequently undergoes necrosis

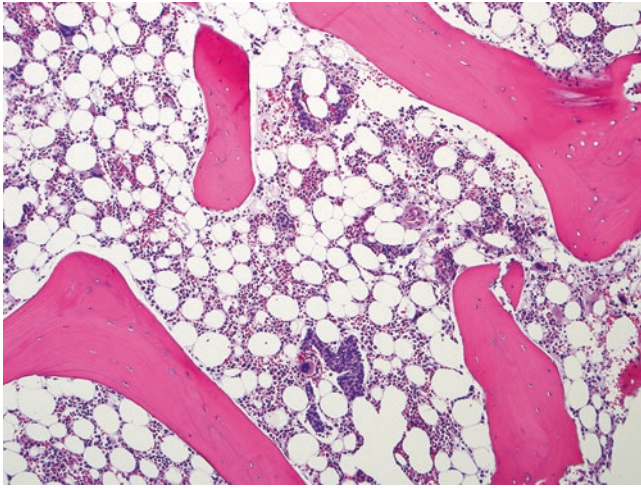


Fig. 18.33 This H&E-stained bone marrow core biopsy shows residual foci of Ewing sarcoma in a child who received intensification chemotherapy. Therapy-related myeloid malignancy has occurred in a subset of patients with refractory Ewing sarcoma treated with intensified chemotherapy

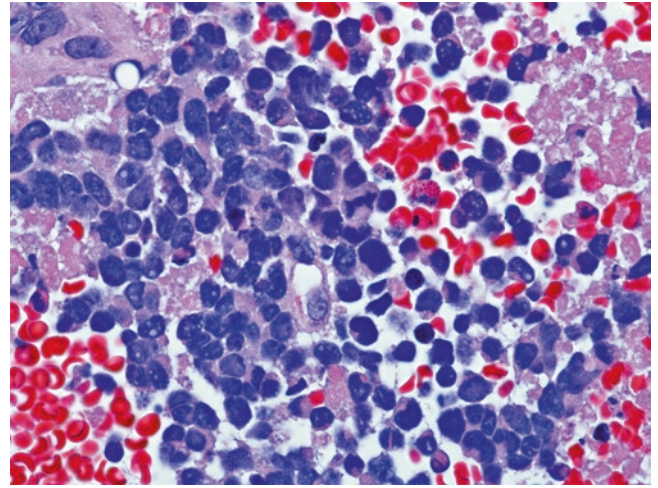


Fig. 18.35 High-power view of the bone marrow clot section involved by poorly differentiated metastatic retinoblastoma. The neoplastic cells are composed of singly distributed tumor cells with high N:C ratio, increased mitoses, and tumor necrosis

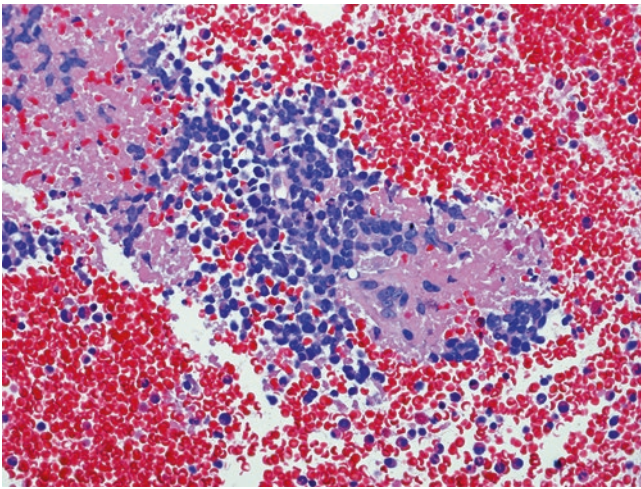


Fig. 18.34 H&E-stained bone marrow clot section from a 3-year-old child with poorly differentiated retinoblastoma of the right eye shows marrow involvement by a small blue-cell tumor, with extensive necrosis consistent with metastatic retinoblastoma. The neoplastic cells expressed neuron-specific enolase and synaptophysin by immunohistochemistry

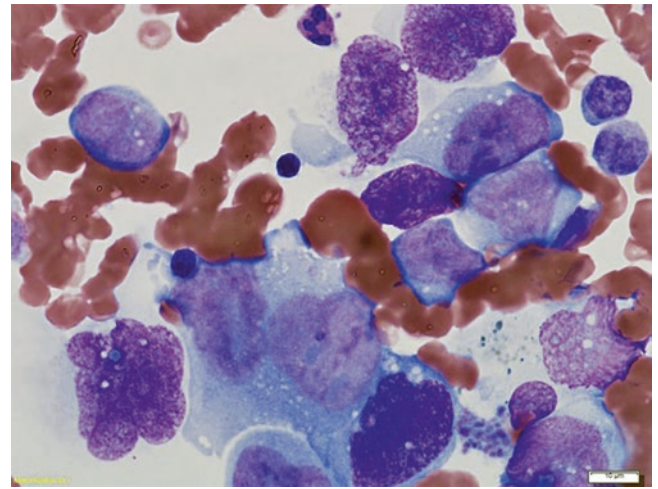


Fig. 18.36 Wright-stained staging bone marrow aspirate smear from a 19-year-old patient with recent diagnosis of testicular alveolar rhabdomyosarcoma shows scattered neoplastic cells, including a bilobed malignant cell with features of a rhabdomyoblast

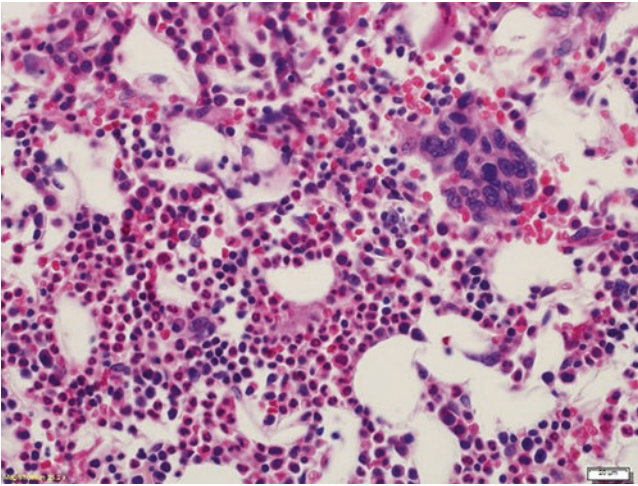


Fig. 18.37 Bone marrow core biopsy reveals a small focus of metastatic rhabdomyosarcoma. The uninvolved bone marrow shows active trilineage hematopoiesis

Suggested Reading

1. Chabot-Richards D, Buehler K, Vasef MA. Detection of EGFR exon 19 E746-A750 deletion and EGFR exon21 point mutations in lung adenocarcinoma by Immunohistochemistry: a comparative study to EGFR exons 19 and 21 mutations analysis using PCR followed by high-resolution melting and pyrosequencing. *J Histotechnol.* 2015;38:56–62.
2. Cotta CV, Konoplev S, Medeiros LJ, Bueso-Ramos CE. Metastatic tumors in bone marrow: histopathology and advances in the biology of the tumor cells and bone marrow environment. *Ann Diagn Pathol.* 2006;10:169–92.
3. Grzywacs B. Metastatic tumors involving bone marrow. In: Foucar K, McKenna RW, Peterson LC, Kroft SH, editors. *Tumors of the bone marrow. AFIP Atlas of Tumor Pathology Series, vol. 4.* Washington, DC: American Registry of Pathology; 2016. p. 787–805.
4. Russell HV, Golding LA, Suell MN, Nuchtern JG, Strother DR. The role of bone marrow evaluation in the staging of the patients with otherwise localized, low-risk neuroblastoma. *Pediatr Blood Cancer.* 2005;45:916–9.

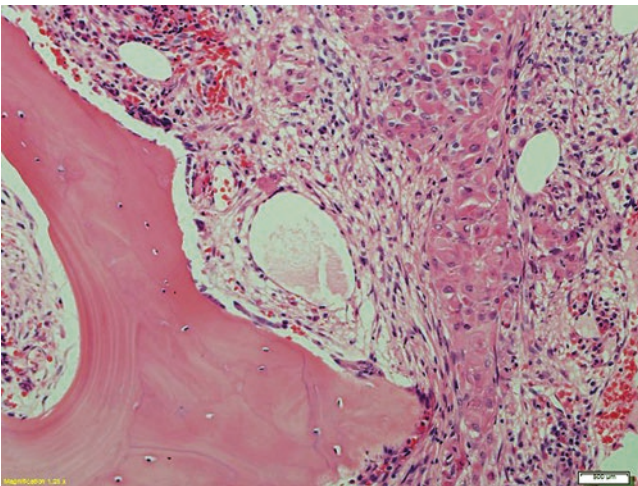


Fig. 18.38 Posttherapy bone marrow trephine biopsy of a patient with extensive marrow involvement by rhabdomyosarcoma reveals patchy foci of residual tumor cells, which have undergone maturation due to tumor response to chemotherapy